The Journal of Chemical Physics

RESEARCH ARTICLE | JUNE 13 2023

Quantitative morphological analysis of InP-based quantum dots reveals new insights into the complexity of shell growth

Special Collection: 40 Years of Colloidal Nanocrystals in JCP

Sophia M. Click ; Alexandra C. Koziel ; Ruben Torres ; Sebastian Flores; James R. McBride ; Sandra J. Rosenthal

J. Chem. Phys. 158, 224705 (2023)
https://doi.org/10.1063/5.0149097

AIP Publishing

The Journal of Chemical Physics ARTICLE scitation.org/journal/jcp

Quantitative morphological analysis of InP-based quantum dots reveals new insights into the complexity of shell growth

Cite as: J. Chem. Phys. 158, 224705 (2023); doi: 10.1063/5.0149097
Submitted: 3 March 2023 • Accepted: 22 May 2023 •
Published Online: 13 June 2023 • Corrected: 16 January 2024

Sophia M. Click,[1,2] Alexandra C. Koziel,[1,2] Ruben Torres,[1,3] Sebastian Flores,[1] James R. McBride,[1,2,a)] and Sandra J. Rosenthal[1,2,3,4,5,a)]

AFFILIATIONS

[1] Department of Chemistry, Vanderbilt University, Nashville, Tennessee 37235, USA
[2] Vanderbilt Institute of Nanoscale Science and Engineering, Vanderbilt University, Nashville, Tennessee 37235, USA
[3] Vanderbilt Institute of Chemical Biology, Vanderbilt University, Nashville, Tennessee 37235, USA
[4] Department of Pharmacology, Vanderbilt University, Nashville, Tennessee 37235, USA
[5] Department of Chemical and Biomolecular Engineering, Vanderbilt University, Nashville, Tennessee 37235, USA

Note: This paper is part of the JCP Special Topic on 40 Years of Colloidal Nanocrystals in JCP.
[a)] **Authors to whom correspondence should be addressed:** james.r.mbbride@vanderbilt.edu and sandra.j.rosenthal@vanderbilt.edu

ABSTRACT

The incorporation of quantum dots in display technology has fueled a renewed interest in InP-based quantum dots, but difficulty controlling the Zn chemistry during shelling has stymied thick, even ZnSe shell growth. The characteristic uneven, lobed morphology of Zn-based shells is difficult to assess qualitatively and measure through traditional methods. Here, we present a methodological study utilizing quantitative morphological analysis of InP/ZnSe quantum dots to analyze the impact of key shelling parameters on InP core passivation and shell epitaxy. We compare conventional hand-drawn measurements with an open-source semi-automated protocol to showcase the improved precision and speed of this method. Additionally, we find that quantitative morphological assessment can discern morphological trends in morphologies that qualitative methods cannot. In conjunction with ensemble fluorescence measurements, we find that changes to shelling parameters that promote even shell growth often do so at the cost of core homogeneity. These results indicate that the chemistry of passivating the core and promoting shell growth must be balanced carefully to maximize brightness while maintaining emission color-purity.

I. INTRODUCTION

Quantum dots (QDs) are semiconductor nanocrystals whose tunable electronic properties make them useful as photon emitters and charge separators in a wide array of applications, including solid state lighting,[1–3] lasing,[4–6] bioimaging,[7–9] 3D printing,[10] luminescent solar concentrators,[11] photovoltaics,[12] and photonic quantum technology.[13,14] QDs have a unique structure-function connection that arises from the quantum confinement of their charge carriers and causes their electronic properties to become dependent on the nanocrystal structure.[15] This dependence is clearly illustrated by the increasing photoluminescent (PL) energy with decreasing QD size.[16] This structure-function dependence causes the QD size, morphology, crystallinity, and surface binding to dictate their electronic properties.[16–20]

Nanocrystal size can be revealed with dynamic light scattering (DLS),[21] atomic force microscopy (AFM),[22] powder x-ray diffraction (XRD),[23] and transmission election microscopy (TEM).[24] The most accurate of these methods is TEM, which can resolve nanocrystal lattice fringes but is limited by electron diffraction contrast convoluting nanocrystal contrast. Scanning transmission electron microscopy (STEM) minimizes diffraction contrast by collecting

only highly scattered electrons. Using an annular electron detector to perform high angle annular dark field (HAADF) imaging provides atomic-number or Z-contrast that can resolve the nanocrystal structure down to columns of individual atoms.[25] Despite the high spatial resolution in STEM and TEM images, analysis methods for extracting nanocrystal size and morphology from STEM and TEM images are either too simplistic, limiting the precision and accuracy of size measurements, or are reliant on computationally constrained approaches that require high quality samples with specific geometries.[26–31]

The simplest methods are limited to rudimentary sizing measurements estimated by hand-drawn particle diameters. These methods are time-consuming and rely only on qualitative descriptions of the morphology set by the individual carrying out the analysis, thus compounding variation with each subsequent analysis. Recently developed automated methods have the advantage of fast, reproducible, high-throughput analysis of both nanocrystal size and morphology but require high quality, uniform samples.[31] Therefore, there is a need to implement an analysis method that can precisely extract size and morphology measurements from electron microscopy images of a wide variety of nanocrystal samples. The open-source image processing software Fiji (Fiji is Just ImageJ) contains a Particle Analysis feature that can be easily adapted to reproducibly extract accurate and precise size and morphological measurements from STEM or bright field TEM images of nanocrystals.[32]

Indium phosphide-based QDs offer a cadmium-free QD alternative whose emission can be tuned throughout the visible spectrum.[33] Recent shifts from ZnS to ZnSe/ZnS shells have produced bright, color-pure samples and opened the floodgates for successful synthetic studies.[3] However, the difficult zinc chemistry often results in uneven shell morphology that is difficult to correlate with PL behavior due to imprecise size and morphological measurements. Precise morphological analysis is needed to elucidate the role of different synthetic conditions on the zinc chemistry to grow thick, uniform Zn-based shells. Here, we present a methodological study combining quantitative morphological analysis of STEM images in Fiji Particle Analysis with trends in ensemble fluorescence of InP/ZnSe QDs to differentiate the impact of key shelling parameters in InP core passivation and ZnSe shell morphology.

II. RESULTS AND DISCUSSION

A. Fiji analysis vs hand analysis

There is a plethora of methods for extracting the nanocrystal size and morphology information from electron microscopy images. The simplest procedures employ hand-drawn cross sections to approximate nanocrystal diameters.[26,27] These procedures are useful because they can easily be applied to almost any sample material, morphology, or heterogeneity, but their simplicity is also their limiting factor. Hand-made length measurements assume particle geometry (i.e., diameter assumes circular or spherical shape) and require qualitative visual assessment to discern morphological trends, and their reliance on human measurements introduces significant error. A recent push to develop precise, high-throughput measurements has produced numerous machine learning and segmentation-based methods to analyze the nanocrystal size and shape.[28–31] Unfortunately, these methods rely on shape classification systems that require relatively uniform, geometrically shaped samples. The

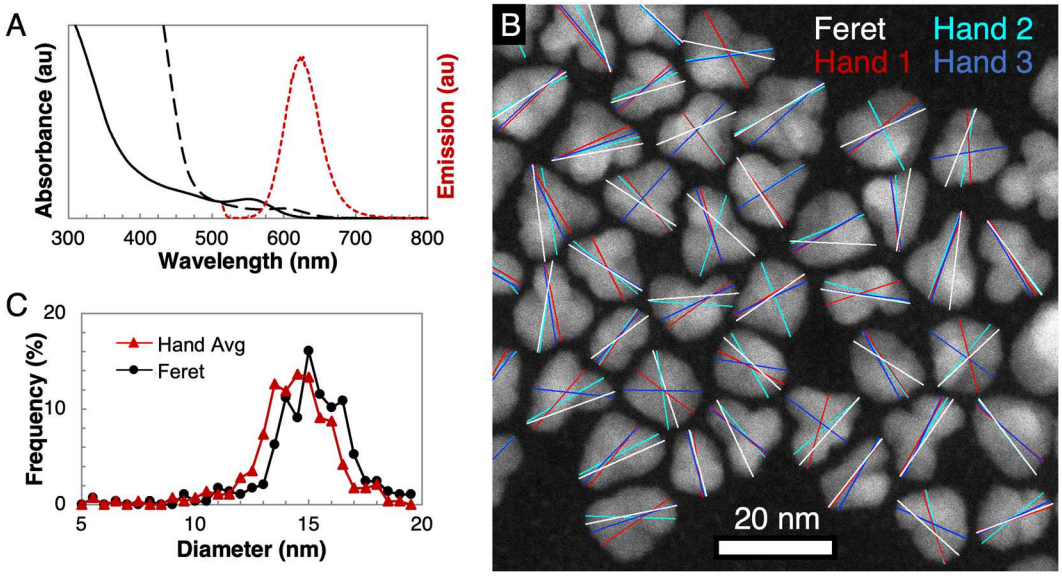

FIG. 1. (a) Absorbance of InP QDs (black), InP/ZnSe QDs (black dashed), and PL of InP/ZnSe QDs (red dashed). (b) STEM image of InP/ZnSe QDs with overlays of hand-drawn diameters (cyan, red, and blue) and Feret diameters (white). Scale bar is 20 nm. (c) Histogram of InP/ZnSe QD hand-drawn diameters (red) and Feret diameters (black).

computational complexity of these methods better suits them to high throughput analysis of well-characterized nanocrystals for quality assessment rather than to morphological characterization of novel nanocrystals produced in a research setting. The Particle Analysis feature in open-source image processing software Fiji combines the precision and reliability of automated procedures with the simplicity and versatility of hand measurements.

To demonstrate the precision and reliability of the Fiji Particle Analysis method, hand measurements taken by three researchers were compared with Fiji Particle Analysis measurements of InP/ZnSe QDs with a lobed shell morphology. InP/ZnSe QDs were synthesized based on a modification of the method developed by Reid *et al.*,[34] utilizing a continuous injection shelling method at 340 °C to grow a thick ZnSe shell on an InP core (~2.4 nm diameter) to produce QDs with a single PL peak centered at 623 nm, a full width at half max (FWHM) of 56 nm, and a photoluminescence quantum yield (PLQY) of 48% [Fig. 1(a)].

For the Fiji Particle Analysis method, particle perimeters of InP/ZnSe QDs were extracted from STEM images using contrast-based manual thresholding and then measured as a function of particle area (nm^2) and Feret diameter (also known as caliper diameter, the longest length between two parallel lines tangential to a particle's silhouette) (see the supplementary material, Text S1). Lower thresholds were used for the smallest nanocrystals (area < 25 nm^2) since their smaller volumes produce lower contrast in HAADF-STEM. All images were subjected to a Gaussian filter of 2 pixels before thresholding to reduce noise. All images analyzed were taken at the same magnification, 630 kx, to maximize analysis resolution. Particle diameters from these same images were independently hand measured by three researchers so that each analyzed particle had three hand-measured diameters, one Feret diameter (i.e., maximum caliper), and one particle area [Fig. 1(b)]. The results of these measurements are summarized in Table I.

At 14.76 nm, the average Feret diameter is 0.7 nm longer than the average hand diameter [Fig. 1(c)]. This result indicates the tendency for hand measurements to underestimate particle diameter. Additionally, the hand diameters for each particle varies an average of 0.8 nm, with measurements on the same particle varying up to 3.7 nm. The lack of precision with hand measurements introduces a significant source of error into the measurement. Combined with the inherent error from using a one-dimensional measurement to describe the size of a three-dimensional particle, the imprecision of hand-measured diameters significantly limits the accuracy of the diameter size measurement. Fiji's Particle Analysis method offers a two-dimensional size measurement, particle area (nm^2), that more accurately reflects the sample size distribution than diameter. Measuring the particle areas reveals an average particle area of 123.85 nm^2 with a mean standard error of 1.58 nm^2 or 1.28% and a standard deviation of 26.77 nm^2 or 21.62%. The standard deviation in the area measurement is significantly larger than the standard deviation of the hand diameters and the Feret diameter, which more

TABLE I. Results summarizing particle analysis measurements (Feret diameter) and hand measurements (diameters 1, 2, 3, and avg) of InP/ZnSe QDs (n = 286).

	Diameter 1	Diameter 2	Diameter 3	Diameter avg	Feret
Analysis time (min)	55	100	98	84	30
Average (nm)	13.8	14.2	14.1	14.1	14.76
Min (nm)	5.1	5.1	5.1	5.1	5.17
Max (nm)	18.8	18.8	19.3	18.7	19.33
Standard deviation (%)	14.1	13.8	13.7	13.5	13.6
Standard error (%)	0.84	0.81	0.81	0.80	1.278

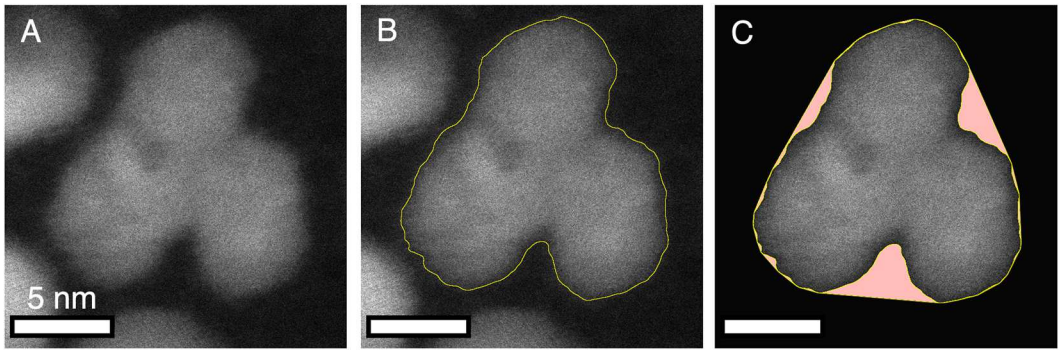

FIG. 2. (a) STEM image of a InP/ZnSe QD. (b) STEM image of the same InP/ZnSe QD with the particle perimeter overlayed. (c) STEM image of the same InP/ZnSe QD with the convex hull overlayed.

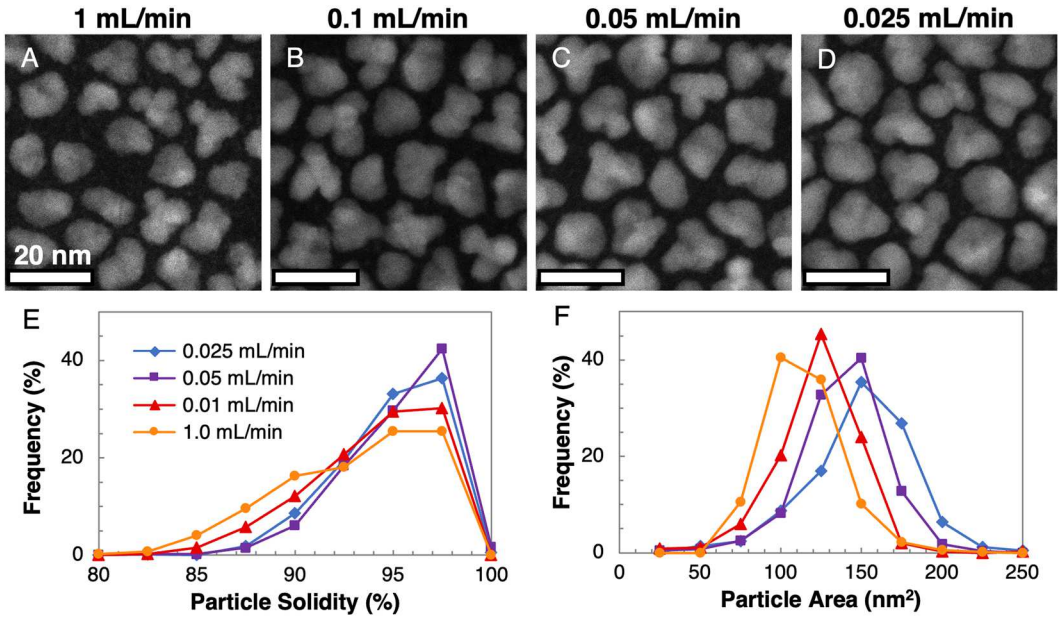

FIG. 3. (a)–(d) STEM images of InP/ZnSe QDs shelled with varied injection rates. (e) Frequency diagrams of solidities of InP/ZnSe QDs shelled with varied injection rates. (f) Frequency diagrams of sizes of InP/ZnSe QDs shelled with varied injection rates. Particle areas and solidities of all four samples have statistically different distributions, with $p < 0.01$ according to the Kolmogorov–Smirnov test.

accurately reflects the uneven shelling that is masked by a single dimensional measurement.

B. Quantitative morphological analysis: Shelling rate

Nanocrystal morphology, in addition to size, is important for photonics, plasmonics, catalysis, and nanomedicine.[20,35–37] Morphology affects these functions by dictating surface area, surface binding, and nanocrystal anisotropy. In core/shell QDs, surface defects, stacking faults, surface roughness, divots, and uneven shell epitaxy have all been shown to reduce PL efficiency by promoting nonradiative exciton recombination pathways.[17,20,38] Despite this clear structure–function correlation, morphological assessments are almost always qualitative visual assessments of electron microscopy images. These qualitative assessments are limited to sweeping generalizations of visually discernible differences or pinpointing specific lattice defects on individual nanocrystals. There is a need for quantitative metrics of nanocrystal morphology to assess global morphological trends. In addition to size measurements, the Fiji Particle Analysis method measures morphological parameters (circularity, roundness, and solidity) that quantitatively describe particle morphology. Of these parameters, solidity offers a quantitative metric to assess variation in shell thickness across a nanocrystal by comparing the area of the particle with the area of its convex hull area (Fig. 2).

To test the ability of solidity to discern particle morphology, we varied the ZnSe shelling injection rate from 1 to 0.025 ml/min. With the decreasing shelling rate, the emission peak red shifted slightly (from 619 to 626 nm) and narrowed (from 61 to 53 nm).

TABLE II. Results of Fiji Particle Analysis of InP/ZnSe QDs synthesized with varying shelling rates.

Rate (ml/min)	1	0.1	0.05	0.025
PLQY (%)	35	44	48	39
Emission peak (nm)	619	623	623	626
Emission FWHM (nm)	61	58	56	53
Area (nm^2)	101.57	110.18	126.75	135.92
Area stdr. error	0.98	1.15	1.11	1.15
Solidity (%)	91.852	92.804	94.048	93.672
Solidity stdr. error (%)	0.156	0.148	0.111	0.091
QDs measured	541	454	545	827

The PLQY increased with the decreasing rate until it peaked at 48% with 0.05 ml/h and dropped to 39% with 0.025 ml/min. Qualitative analysis of STEM images of the samples reveals a general trend of increasing size and more even morphology as the shelling rate was decreased, but all samples display particles with divots and lobed shell growth that are difficult to differentiate between shell rates [Figs. 3(a)–3(d)]. Fiji Particle Analysis on these same images finds that the average particle area increased from 101.57 to 135.92 nm^2 with the decreasing shelling rate (Table II). Despite the samples having qualitatively similar morphologies, all four samples have

TABLE III. Results of Fiji Particle Analysis of InP/ZnSe QDs synthesized with varying shelling temperatures.

Temperature (°C)	320 °C	340 °C	360 °C
PLQY (%)	41	47	23
Emission peak (nm)	600	610	624
Emission FWHM (nm)	43	45	47
Area (nm^2)	106.64	137.89	141.43
Area stdr. error (nm^2)	1.40	1.46	3.11
Solidity (%)	93.859	95.585	95.263
Solidity stdr. error (%)	0.097	0.067	0.119
QDs measured	660	579	441

statistically different solidity distributions, with $p < 0.01$ according to both the Kolmogorov–Smirnov test and Mann–Whitney test. Matching the PLQY trend, the InP/ZnSe QDs shelled at 0.05 ml/min have the highest average solidity and the smallest size distribution, indicating a more even shelling morphology that would otherwise be indiscernible. A closer look at the distribution of solidities reveals a subpopulation of lower solidity particles that shifts toward higher solidities with the decreasing shelling rate until 0.05 ml/min [Fig. 3(e)]. Furthermore, analysis of the size distributions does not reveal this same trend [Fig. 3(f)], indicating the need for morphological measurements in addition to size measurements to fully assess nanocrystals.

C. Quantitative morphological analysis: Shelling temperature

Next, we investigated the role of shelling temperature on shell morphology. It has been shown that increasing Zn shelling temperatures from 300 to 340 °C produces InP/ZnSe/ZnS QDs with more even shell coverage and higher PLQY.[3,39] A quantitative morphological analysis of this trend can further dissect the roll of shell coverage to differentiate between shell morphology and core passivation. Ensemble fluorescent measurements indicate how changes to the core surface during initial monolayers of shell growth affect core passivation. By comparing trends in fluorescence properties with morphological changes, we can evaluate how

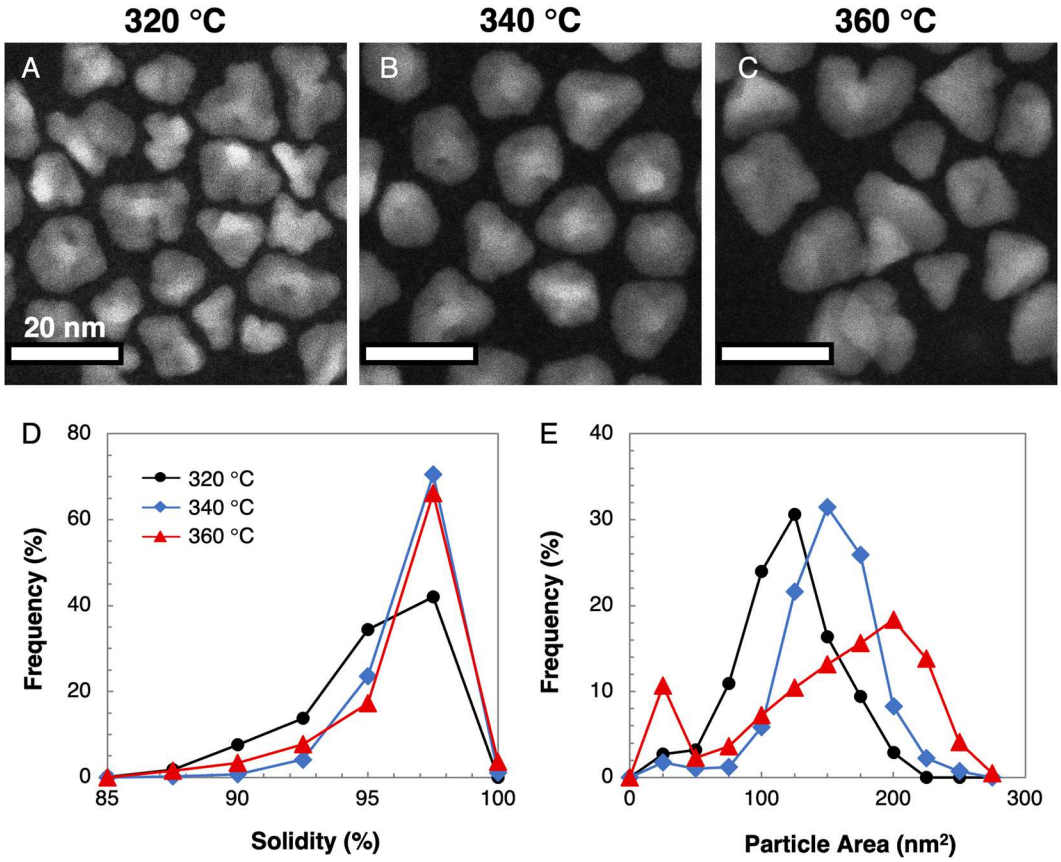

FIG. 4. (a)–(c) STEM images of InP/ZnSe QDs shelled at varied temperatures. (d) Frequency diagram of solidities of InP/ZnSe QDs shelled at varied temperatures. (e) Frequency diagram of sizes of InP/ZnSe QDs shelled at varied temperatures. Particle areas and solidities of all three samples have statistically different distributions, with $p < 0.01$ according to the Kolmogorov–Smirnov test.

TABLE IV. Results of Fiji Particle Analysis of InP/ZnSe QDs synthesized with varying amines.

	OLA	DOA	TOA	No amine
PLQY (%)	25	25	25	21
Emission peak (nm)	625	624	624	625
Emission FWHM (nm)	81	70	62	61
Area (nm^2)	90.6	132.3	116.9	123.0
Area stdr. error (nm^2)	1.9	2.1	2.9	2.9
Solidity (%)	93.85	95.65	94.90	95.27
Solidity stdr. error (%)	0.19	0.11	0.13	0.13
QDs measured	219	285	216	295

shelling conditions affect core surface chemistry and epitaxial shell growth.

InP/ZnSe QDs were shelled at 320, 340, and 360 °C to assess how the increased shelling temperature affects shell growth. The results are summarized in Table III. Increasing the shelling temperature from 320 to 360 °C red shifts the ensemble emission peak from 600 to 624 nm while also broadening the emission peak from 43 to 47 nm FWHM. The reduced confinement due to the ZnSe band gap is expected to cause red shifting with the first few monolayers of ZnSe deposition, but since these samples all have thick shells (>5 nm), this indicates a change in core size.[40] Fiji Particle Analysis on STEM images of these samples reveals increasing particle size from 106.64 to 141.43 nm^2 with increasing shelling temperature from 320 to 360 °C [Figs. 4(a)–4(c)]. The increased temperature likely causes *in situ* defocusing and ripening of the InP core. The PLQY increases slightly from 41 to 47% with the temperature increasing from 320 to 340 °C and then drops significantly to 23% during the 360 °C shelling. This drop in PLQY signifies a change in core passivation, which may be due to ligand decomposition from the high temperature.

Shelling at higher temperatures (340 and 360 °C) significantly increases the average particle solidity, but the distribution of sizes and solidities for the 360 °C shelling are significantly broader than for the 340 °C shelling [Figs. 4(d) and 4(e)]. The increase in size distribution paired with the high solidity and the 360 °C shelling indicates that the better control of the Zn chemistry afforded at higher temperatures is being countered by less effective core passivation that reduces PLQY.

D. Quantitative morphological analysis: Ligand effects

Trioctylamine (TOA) is commonly used as both the surfactant and solvent for high temperature shellings (>300 °C) due to its high boiling point, ease of use, and purported shape control at 340 °C.[3] To test the role of amine sterics on particle shape control, TOA was exchanged for several other amines, including a secondary amine dioctylamine (DOA), a primary amine oleylamine (OLA), and a non-coordinating amine octadecene (ODE). Long-chain amines were chosen for their high boiling points, but the annealing temperatures still had to be reduced to 300 °C to accommodate the lower boiling point of dioctylamine (~298 °C). Increasing the steric bulk of the amine from primary to secondary to tertiary maintained the PLQY and emission peak energy of the InP/ZnSe QDs but

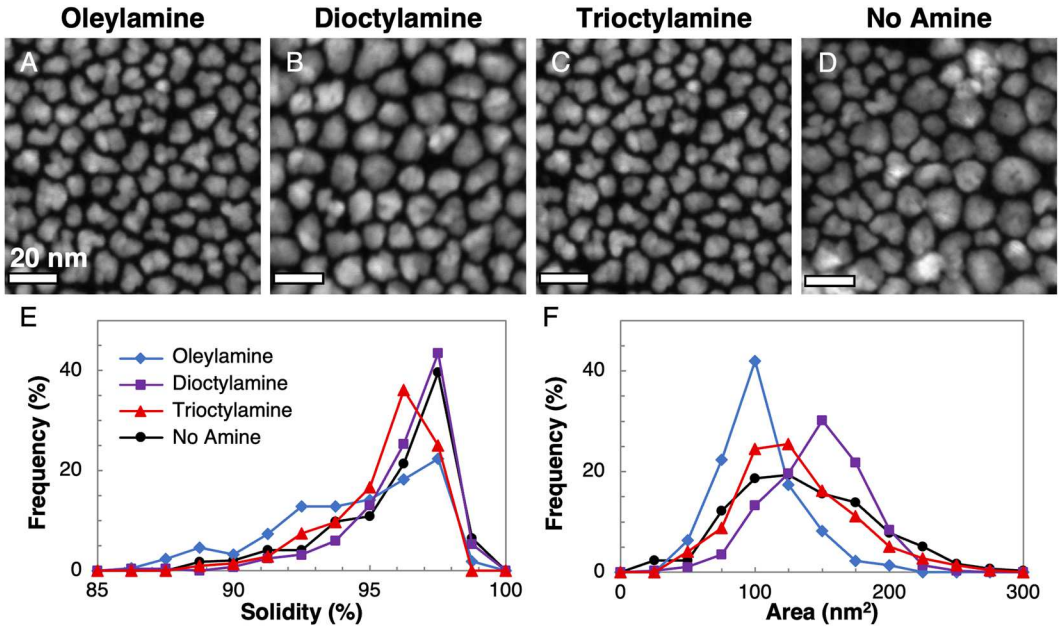

FIG. 5. (a)–(d) STEM images of InP/ZnSe QDs shelled with varied injection rates. (e) Frequency diagram of solidities of InP/ZnSe QDs shelled with varied injection rates. (f) Frequency diagram of sizes of InP/ZnSe QDs shelled with varied injection rates. Particle areas and solidities of all four samples have statistically different distributions, with $p \ll 0.001$ according to the Kolmogorov–Smirnov test, except for the solidities of DOA and No amine ($p < 0.1$) and the areas of TOA and No amine ($p < 0.5$).

decreased the emission energy line width. Fiji Particle Analysis, summarized in Table IV, reveals that dioctylamine produced the thickest shells with the smallest size distribution and most even morphology, oleylamine produced the thinnest shells with the most uneven morphology, and trioctylamine broadened the size distribution despite suppressing emission line widths [Figs. 5(a)–5(f)]. Increasing the shelling temperature to 340 °C with trioctylamine improves the size distribution and shell morphology similar to using dioctylamine at 300 °C (see the supplementary material, Fig. S1). Replacing the amine with non-coordinating octadecene resulted in the lowest line width but the largest size distribution. While these findings initially seem at odds, they highlight how synthetic conditions during shelling affect both the core QD and the epitaxial shell growth. In this case, the basicity of the amines likely causes etching of the InP cores during heat up and initial shell growth, causing increased ensemble heterogeneity via Ostwald-like ripening that increases the ensemble line widths. Once a thin ZnSe layer is deposited, the amines interact with the shell material, acting as ligands to facilitate further shell growth and final shell morphology. Although the etched cores display broader linewidths, the etching may also remove oxidized surface atoms, creating a more even surface for more uniform shell growth that reduces the final size distribution of the InP/ZnSe QDs.

III. CONCLUSIONS

We have reported the use of quantitative morphological measurements to discern variations in InP/ZnSe QDs and elucidate the effects of synthetic parameters on shell growth. Using the semi-automated Particle Analysis protocol in the open-source image processing software Fiji to extract particle perimeters from STEM images provides more precise size measurements than traditional hand-drawn diameter measurements. Furthermore, measuring nanocrystal size as a function of area within the perimeter more accurately reflects sample heterogeneity that is masked by the one-dimensional diameter measurement. The Particle Analysis protocol also provides quantitative morphological parameters that can reproducibly find morphological variations that qualitative analysis cannot discern. Combined, quantitative morphological analysis with fluorescence measurements discerns how changes in synthetic shelling conditions can deleteriously etch the unprotected InP core yet simultaneously increase even shell epitaxy.

IV. EXPERIMENTAL SECTION

A. Chemicals

Indium (III) acetate (99.99%, trace metals basis), zinc acetate (99.99%, trace metal basis), tris(trimethylsilyl)phosphine (95%), myristic acid (99%), oleic acid (90%, technical grade), 1-octadecene (ODE, 90%, technical grade), oleylamine (OLA, 70%, technical grade), dioctylamine (DOA, 98%) trioctylphosphine (TOP, 97%), acetonitrile (99.8%, anhydrous), and molecular sieves (4A, beads, 8–12 mesh) were obtained from Aldrich. Tri-*n*-octylamine (TOA, 97%) was obtained from Acros Organics. Selenium powder (99.99%, 200 mesh) was obtained from Alfa Aesar. Sulfur powder (99.99%), isopropanol (99.9%), hexanes (99.9%), and toluene (99.9%) were obtained from Fisher Scientific.

Solvents (octadecene, oleylamine, dioctylamine, acetonitrile, isopropanol, and toluene) were subjected to three cycles of freeze–pump–thaw cycling with liquid nitrogen and high vacuum to remove dissolved gasses before storing in a nitrogen glovebox over sieves.

All other chemicals were used without further purification unless noted otherwise.

B. Precursor preparation

Indium myristate ($InMy_3$) was prepared following a similar literature protocol by degassing 1.4595 g (5 mmol) indium acetate, 4.1109 g myristic acid, 50 ml ODE in a 100 ml three-neck round-bottom flask on a Schlenk line at 110 °C under vacuum for 1 h. The reaction was then placed under an argon atmosphere and heated to 150 °C for 30 min, until the solution became clear. The solution was then further degassed at 110 °C under vacuum for 1 h before being placed back under an argon atmosphere and cooling to room temperature. The white precipitate was vacuum filtered using a M frit funnel and washed with hexanes and deionized water before being transferred to a tared vial, dried under vacuum overnight, and then stored in a desiccator. ^{1}H NMR of precipitate NMR of precipitate was performed on a Bruker 400 MHz console equipped with an 9.4 T Oxford magnet with 5 mm Z-gradient broadband (BBFO) probe with automatic tuning and matching capability (ATM). It was prepared in deuterated toluene and found full conversion to $InMy_3$ with no acetic acid or water present (see the supplementary material, Fig. S2).

$InMy_3TOP_3$ (0.2M) was prepared by degassing 3.1920 g (4 mmol) $InMy_3$ and 15 ml ODE in a 100 ml three-neck round-bottom flask on a Schlenk line at 120 °C under vacuum for 2 h. The solution was then placed under an argon atmosphere and 5.3 ml (12 mmol) TOP was injected and annealed for 30 min before being cooled to room temperature. The solution was subjected to three cycles of freeze–pump–thawing to remove dissolved gasses before storing in a nitrogen glovebox.

Zinc oleate (0.4M) was prepared by degassing 2.57 g (14 mmol) of zinc acetate, 9 ml of oleic acid, and 26 ml TOA in a 100 ml three-neck round-bottom flask on a Schlenk line at 120 °C under vacuum for 2 h. The reaction was then placed under an argon atmosphere and heated to 280 °C before further degassing at 120 °C under vacuum for 30 min. The solution was placed back under an argon atmosphere, cooled to room temperature, and then subjected to three cycles of freeze–pump–thawing to remove dissolved gasses before storing in a nitrogen glovebox.

TOP-Se (0.4M) was prepared by dissolving 0.95 g (12 mmol) of selenium powder in 30 ml TOP with stirring until completely dissolved in a nitrogen-filled glovebox.

TOP-S (0.4M) was prepared by heating 0.38 g (12 mmol) of sulfur in 30 ml TOP with stirring until completely dissolved in a nitrogen-filled glovebox.

C. InP QD synthesis

InP QD cores were synthesized using a modified literature protocol.[26] Briefly, 1.0 ml (0.2 mmol) $InMy_3TOP_3$ and 4 ml ODE were added to a 50 ml three-neck round-bottom flask in a nitrogen-filled glovebox. The mixture was put under an argon

atmosphere and heated to 150 °C with stirring for 30 min. The reaction was then heated to 270 °C. A solution of 30 μl (0.1 mmol) tris(trimethylsilyl)phosphine [$(TMS)_3P$] and 1 ml TOP or ODE was quickly injected into the reaction flask and the QDs grown for 30 minutes before cooling to room temperature. The nanocrystals were purified via centrifugation at 8000 rpm for 10 min with isopropanol and redispersed in toluene. The InP QDs obtained were typically 2.5 nm in diameter.

D. InP/ZnSe QD synthesis

InP QDs were synthesized as described above and stored in a nitrogen glovebox. Shell growth was performed using a modified literature procedure.[34] In a nitrogen glovebox, 6 ml TOA was added into a 100 ml three-neck round-bottom flask. The solution was then put under an argon atmosphere and heated to 150 °C. A mixture of 150 nmol InP QDs and 0.1 mmol Zn oleate was injected and heated to 340 °C, QD concentration calculated according to Achorn *et al.* and Talapin *et al.*[41,42] A mixture of zinc oleate (2 ml, 0.4M. stock) and Se-TOP (2 ml, 0.4M stock) was added dropwise into the growth solution at a rate of 1.5 ml/h for 2 h using a syringe pump. The reaction solution was further annealed at 340 °C for 30 min. After cooling to room temperature, the crude InP–ZnSe core-shell stock was stored in a nitrogen glovebox. Samples for optical and structural characterization were prepared by centrifuging at 10 000 rpm for 10 min with isopropanol and re-dispersing in toluene.

E. InP/ZnSe/ZnS QD synthesis

InP QDs were synthesized and shelled with ZnSe as described above. Once the ZnSe continuous injection was complete, the reaction was further annealed for 10 min at 340 °C. A mixture of zinc oleate (1 ml, 0.4M stock) and S-TOP (1 ml, 0.4M stock) was added dropwise into the growth solution at a rate of 1.5 ml/h for 30 min using a syringe pump. The reaction was further annealed at 340 °C for 30 min. After cooling to room temperature, the crude InP–ZnSe core-shell stock was stored in a nitrogen glovebox. Samples for optical and structural characterization were prepared by centrifuging at 10 000 rpm for 10 min with isopropanol and re-dispersing in toluene.

F. Ensemble spectroscopy

Absorption spectra were recorded on a Cary 60 UV–VIS spectrometer. Photoluminescence (PL) spectra were collected on a PTI QuantaMaster fluorescence spectrophotometer using a 75 W Xe arc lamp as the excitation source. PL was measured with a 1 s integration time and a 1 nm slit width. Photoluminescent quantum yield (PLQY) measurements were determined by comparing the integrated emission intensities of the QDs with a reference dye (R610 in ethanol, QY ~ 71%) according to IUPAC standards using an excitation wavelength of 500 nm and optical density (OD) of ~0.1 for all samples.[43]

G. Scanning transmission electron microscopy (STEM) imaging

High resolution scanning transmission electron (HRSTEM) images were obtained using a Tecnai Osiris TEM/STEM operating at 200 kV equipped with a SuperXTM quad EDS detection system. TEM samples were baked at 150 °C under high vacuum prior to imaging. Nanocrystal sizes were determined from STEM images (>500 kx) using the Particle Analysis protocol in the open-source software Fiji (procedure detailed in the supplementary material).[32]

SUPPLEMENTARY MATERIAL

See the supplementary material for the description of the Fiji Particle Analysis procedure and troubleshooting, additional Particle Analysis measurements, and characteristic ^{1}H NMR and FTIR of synthesized indium myristate.

ACKNOWLEDGMENTS

This work was supported by the National Science Foundation CHE (Grant No. 2003310) and the Vanderbilt Institute of Nanoscale Science and Engineering (VINSE).

AUTHOR DECLARATIONS

Conflict of Interest

The authors have no conflicts to disclose.

Author Contributions

The manuscript was written through contributions of all authors. All authors have given approval to the final version of the manuscript.

Sophia M. Click: Conceptualization (lead); Formal analysis (lead); Investigation (lead); Writing – original draft (lead). **Alexandra C. Koziel**: Investigation (supporting); Writing – review & editing (equal). **Ruben Torres**: Investigation (supporting); Writing – review & editing (equal). **Sebastian Flores**: Investigation (equal). **James R. McBride**: Funding acquisition (equal); Writing – review & editing (equal). **Sandra J. Rosenthal**: Funding acquisition (equal); Project administration (equal); Supervision (lead); Writing – review & editing (equal).

DATA AVAILABILITY

The data that support the findings of this study are available from the corresponding authors upon reasonable request.

REFERENCES

[1] Y. Shirasaki, G. J. Supran, M. G. Bawendi, and V. Bulović, Nat. Photonics **7**, 13 (2013).
[2] M. A. Schreuder, K. Xiao, I. N. Ivanov, S. M. Weiss, and S. J. Rosenthal, Nano Lett. **10**, 573 (2010).
[3] Y.-H. Won, O. Cho, T. Kim, D.-Y. Chung, T. Kim, H. Chung, H. Jang, J. Lee, D. Kim, and E. Jang, Nature **575**, 634 (2019).
[4] F. Fan, O. Voznyy, R. P. Sabatini, K. T. Bicanic, M. M. Adachi, J. R. McBride, K. R. Reid, Y.-S. Park, X. Li, A. Jain, R. Quintero-Bermudez, M. Saravanapavanantham, M. Liu, M. Korkusinski, P. Hawrylak, V. I. Klimov, S. J. Rosenthal, S. Hoogland, and E. H. Sargent, Nature **544**, 75 (2017).

[5]D. A. Hanifi, N. D. Bronstein, B. A. Koscher, Z. Nett, J. K. Swabeck, K. Takano, A. M. Schwartzberg, L. Maserati, K. Vandewal, Y. van de Burgt, A. Salleo, and A. P. Alivisatos, Science **363**, 1199 (2019).
[6]Y.-S. Park, J. Roh, B. T. Diroll, R. D. Schaller, and V. I. Klimov, Nat. Rev. Mater. **6**, 382 (2021).
[7]O. Kovtun, I. D. Tomlinson, R. S. Ferguson, and S. J. Rosenthal, PLoS One **14**, e0225339 (2019).
[8]L. B. Thal, V. R. Mann, D. Sprinzen, J. R. McBride, K. R. Reid, I. D. Tomlinson, D. G. McMahon, B. E. Cohen, and S. J. Rosenthal, Biomater. Sci. **8**, 837 (2020).
[9]O. Kovtun, R. Torres, R. S. Ferguson, T. Josephs, and S. J. Rosenthal, Biochemistry **60**, 1031 (2021).
[10]C. D. Brubaker, T. M. Frecker, J. R. McBride, K. R. Reid, G. K. Jennings, S. J. Rosenthal, and D. E. Adams, J. Mater. Chem. C **6**, 7584 (2018).
[11]N. S. Makarov, D. Korus, D. Freppon, K. Ramasamy, D. W. Houck, A. Velarde, A. Parameswar, M. R. Bergren, and H. McDaniel, ACS Appl. Mater. Interfaces **14**, 29679 (2022).
[12]J. S. Niezgoda, A. Ng, J. D. Poplawsky, J. R. McBride, S. J. Pennycook, and S. J. Rosenthal, Adv. Funct. Mater. **26**, 895 (2016).
[13]I. Aharonovich, D. Englund, and M. Toth, Nat. Photonics **10**, 631 (2016).
[14]H. A. Nguyen, D. Sharp, J. E. Fröch, Y.-Y. Cai, S. Wu, M. Monahan, C. Munley, A. Manna, A. Majumdar, C. R. Kagan, and B. M. Cossairt, ACS Appl. Mater. Interfaces **15**, 4294 (2023).
[15]M. G. Bawendi, M. L. Steigerwald, and L. E. Brus, Annu. Rev. Phys. Chem. **41**, 477 (1990).
[16]X. Peng, J. Wickham, and A. P. Alivisatos, J. Am. Chem. Soc. **120**, 5343 (1998).
[17]N. J. Orfield, J. R. McBride, J. D. Keene, L. M. Davis, and S. J. Rosenthal, ACS Nano **9**, 831 (2015).
[18]J. D. Keene, J. R. McBride, N. J. Orfield, and S. J. Rosenthal, ACS Nano **8**, 10665 (2014).
[19]J. R. McBride, N. Mishra, S. M. Click, N. J. Orfield, F. Wang, K. Acharya, M. F. Chisholm, H. Htoon, S. J. Rosenthal, and J. A. Hollingsworth, J. Chem. Phys. **152**, 124713 (2020).
[20]K. R. Reid, J. R. McBride, A. D. la Croix, N. J. Freymeyer, S. M. Click, J. E. Macdonald, and S. J. Rosenthal, ACS Nano **12**, 11434 (2018).
[21]B. N. Khlebtsov and N. G. Khlebtsov, Colloid J. **73**, 118 (2011).
[22]R. D. Boyd, S. K. Pichaimuthu, and A. Cuenat, Colloids Surf., A **387**, 35 (2011).
[23]G. A. Dorofeev, A. N. Streletskii, I. v. Povstugar, A. v. Protasov, and E. P. Elsukov, Colloid J. **74**, 675 (2012).
[24]W. D. Pyrz and D. J. Buttrey, Langmuir **24**, 11350 (2008).
[25]J. R. McBride and S. J. Rosenthal, J. Chem. Phys. **151**, 160903 (2019).
[26]Z. Xu, Y. Li, J. Li, C. Pu, J. Zhou, L. Lv, and X. Peng, Chem. Mater. **31**, 5331 (2019).
[27]C. Shen, Y. Zhu, Z. Li, J. Li, H. Tao, J. Zou, X. Xu, and G. Xu, J. Mater. Chem. C **9**, 9599 (2021).
[28]H. Wen, X. Xu, S. Cheong, S.-C. Lo, J.-H. Chen, S. L. Y. Chang, and C. Dwyer, Nanoscale Adv. **3**, 6956 (2021).
[29]Z. Sun, J. Shi, J. Wang, M. Jiang, Z. Wang, X. Bai, and X. Wang, Nanoscale **14**, 10761 (2022).
[30]K. M. Saaim, S. K. Afridi, M. Nisar, and S. Islam, Ultramicroscopy **233**, 113437 (2022).
[31]B. Lee, S. Yoon, J. W. Lee, Y. Kim, J. Chang, J. Yun, J. C. Ro, J.-S. Lee, and J. H. Lee, ACS Nano **14**, 17125 (2020).
[32]J. Schindelin, I. Arganda-Carreras, E. Frise, V. Kaynig, M. Longair, T. Pietzsch, S. Preibisch, C. Rueden, S. Saalfeld, B. Schmid, J.-Y. Tinevez, D. J. White, V. Hartenstein, K. Eliceiri, P. Tomancak, and A. Cardona, Nat. Methods **9**, 676 (2012).
[33]R. Xie, D. Battaglia, and X. Peng, J. Am. Chem. Soc. **129**, 15432 (2007).
[34]K. R. Reid, J. R. McBride, N. J. Freymeyer, L. B. Thal, and S. J. Rosenthal, Nano Lett. **18**, 709 (2018).
[35]K. Yu, K. L. Kelly, N. Sakai, and T. Tatsuma, Langmuir **24**, 5849 (2008).
[36]M. Periyasamy and A. Kar, J. Mater. Chem. C **8**, 4604 (2020).
[37]J. E. Gagner, M. D. Lopez, J. S. Dordick, and R. W. Siegel, Biomaterials **32**, 7241 (2011).
[38]N. J. Orfield, J. R. McBride, F. Wang, M. R. Buck, J. D. Keene, K. R. Reid, H. Htoon, J. A. Hollingsworth, and S. J. Rosenthal, ACS Nano **10**, 1960 (2016).
[39]J. Park, Y. H. Won, Y. Han, H. M. Kim, E. Jang, and D. Kim, Small **18**, 2105492 (2022).
[40]R. Toufanian, A. Piryatinski, A. H. Mahler, R. Iyer, J. A. Hollingsworth, and A. M. Dennis, Front. Chem. **6**, 567 (2018).
[41]O. B. Achorn, D. Franke, and M. G. Bawendi, Chem. Mater. **32**, 6532 (2020).
[42]D. V. Talapin, "Experimental and theoretical studies on the formation of highly luminescent II-VI, III-V and core-shell semiconductor nanocrystals," Ph.D. dissertation (University of Hamburg, 2002).
[43]A. M. Brouwer, Pure Appl. Chem. **83**, 2213 (2011).